



## Research paper

# One-step hydrothermal synthesis of Bi-TiO<sub>2</sub> nanotube/graphene composites: An efficient photocatalyst for spectacular degradation of organic pollutants under visible light irradiation

Umair Alam <sup>a</sup>, M. Fleisch <sup>b</sup>, Imme Kretschmer <sup>b</sup>, Detlef Bahnemann <sup>b,c</sup>, M. Muneer <sup>a,\*</sup><sup>a</sup> Department of Chemistry, Aligarh Muslim University, Aligarh, 202002, India<sup>b</sup> Photocatalysis and Nanotechnology, Institut fuer Technische Chemie, Gottfried Wilhelm Leibniz Universitaet Hannover, Callinstrasse 3, D-30167 Hannover, Germany<sup>c</sup> Photoactive nanocomposite materials, Saint-Petersburg State University, Ulyanovskaya Str, Peterhof, Saint-Petersburg, 198504, Russia

## ARTICLE INFO

## Article history:

Received 12 February 2017

Received in revised form 1 June 2017

Accepted 5 June 2017

Available online 7 June 2017

## Keywords:

Bi-TiO<sub>2</sub>NT/graphene

Photocatalytic activity

Methylene blue

Dinoseb

## ABSTRACT

In the present study, we have adopted a simple one-pot alkaline hydrothermal route to synthesize Bi-doped TiO<sub>2</sub>NT/graphene composites by using different wt% of Bi with an aim to achieve the excellent photocatalytic activity under visible light source. The nature of GO is changed to deoxygenated graphene with simultaneous embedding of Bi into TiO<sub>2</sub> nanotube (TNT), during hydrothermal process. XRD and FTIR analysis confirm the successful conversion of GO to deoxygenated graphene. EPR analysis reveals the co-existence of Ti<sup>3+</sup> ion with oxygen vacancy, which is created by the Bi doping. The photocatalytic activity of the prepared samples is measured by the degradation of aqueous suspensions of methylene blue (MB) and Dinoseb (phenolic herbicide), under visible-light irradiation. The prepared TiO<sub>2</sub>NT/graphene composite with 2-wt% bismuth (2-BTNTG) has shown the improved photocatalytic activity as compared to their counterparts. The improved photocatalytic activity is associated to the synergistic effect of graphene and Bi-TNT, which facilitate the interfacial charge transfer and enhances the efficiency of light harvesting in the visible region. Moreover, the underlying mechanism involving photocatalytic degradation of organic pollutants over 2-BTNTG is explored by using trapping experiments, suggesting that the ·OH radicals solely contributed to degradation.

© 2017 Published by Elsevier B.V.

## 1. Introduction

Recently, a wide variety of organic pollutants comprising of herbicide derivatives, textile dyes, and phenolic compound derivatives responsible for environmental and water pollution are reported [1–3]. Among these, herbicide derivatives and textiles dyes are most difficult to decompose owing to their chemical and biological stability [4–7]. These are ranked as the most carcinogenic and high toxic pollutants, manifesting the major threat to human and aquatic life [8–10]. Enormous research efforts are devoted to reduce these pollutants in water by biological and physical techniques but the majority of these are cumbersome, expensive and less effective [11–13]. In this regard, semiconductor photocatalysis is emerging as an advanced and green technology for the degradation

of these pollutants due to its environmental benignancy, stability, and safety [14,15]. Significantly, TiO<sub>2</sub> has proven to be one of the most widely accepted and benchmark photocatalytic material owing to its strong oxidizing power, intoxicate high photostability, and low cost [16–19]. One-dimensional (1D) nanostructures of TiO<sub>2</sub>, such as nanorods [20], nanowires [21], and nanotubes [22,23], have gained interest owing to their quantum confinement and high surface area. TiO<sub>2</sub> nanotubes are widely applied in the photocatalytic degradation of organic pollutants because of their structure dependent enhanced photocatalytic properties [23–25]. However, the major drawbacks that confine its use to larger scale are its wide bandgap and quick recombination of charge carriers [25–27]. Several strategies are adopted to modify TiO<sub>2</sub> such as extending its spectral response to the visible region and prolonging the life span of photoinduced electron-hole pairs. The strategies involve, doping with metals and non-metals [27–29], noble metals deposition [30] and heterostructure construction with narrow bandgap semiconductors and carbonaceous materials [31–35]. The carbon-titania nanocomposites by linking titania with carbonaceous materials

\* Corresponding author.

E-mail addresses: [readermuneer@gmail.com](mailto:readermuneer@gmail.com), [m.muneer.ch@amu.ac.in](mailto:m.muneer.ch@amu.ac.in)  
(M. Muneer).

have received much attention as a new class of photocatalysts, which could boost its photocatalytic activity by separating charge carriers and electron transfer from TiO<sub>2</sub> to carbonaceous materials on irradiation [33–38].

Graphene is also used as most suitable two-dimensional nanosheet photocatalyst in the arena of photocatalysis owing to its high surface and superior electron mobility [39–41]. The excited electrons from the semiconductor materials are effectively trapped by the graphene, which hinders the recombination process ultimately enhancing the photocatalytic activity [35,36,38]. In literature, the intimate contact between graphene and TiO<sub>2</sub> has immensely improved the photocatalytic activity because of their π-conjugation system and 2D planar structure. This tends dye molecules to adsorb on their surface more easily through π–π stacking between aromatic regions of graphene and dye molecules [42,43].

Nevertheless, some problem still restrains further promotion of efficiency of the present graphene-based TiO<sub>2</sub> nanocomposites, i.e. weakening of light harvesting efficacy of catalyst which results in the generation of the small fraction of charge carriers, consequently impairing the photocatalytic activity. In order to make full use of solar energy and further alleviate the recombination rate of charge carriers, metal ions doping is found as the most effective way to satiate the above conditions and thus promote the photocatalytic reactions. For instance, Nguyen-phan group has developed a hydrothermal method to synthesize Sn-doped TiO<sub>2</sub> nanoparticles supported onto reduced graphene oxide (rGO) with superior photocatalytic activity [44]. Qian and his co-workers have reported the synthesis of N-doped TiO<sub>2</sub>/graphene composites with prolonged electron life time for high-performance photocatalytic degradation due to the synergistic action of graphene and N-doped TiO<sub>2</sub> [45]. Chen et al. have reported the synthesis of Mn-doped TiO<sub>2</sub> grown on graphene via one-pot hydrothermal method, which showed the highest photocatalytic activity for the removal of Cr(VI) and Cr(III) under sunlight [46]. These researches reveal that the simultaneous incorporation of graphene and metal ions can significantly improve the photocatalytic activity of semiconducting materials to the larger extent.

In recent years most of the researches are inclined to the formation of bismuth-doped TiO<sub>2</sub> nanostructures via hydrothermal method, which can improve the photocatalytic activity for the removal of organic pollutants owing to its ability to take advantage of the broad range of solar spectrum [47–50]. Bismuth-doped TiO<sub>2</sub> nanofibers are prepared by an alkaline hydrothermal approach that showed the structure dependent enhanced photocatalytic activity for hydrogen production as well as MO degradation under both UV and visible light irradiation [51]. A literature reported on the synthesis of bismuth doped TiO<sub>2</sub> hollow thin sheet with enhanced photocatalytic activity towards the decomposition of different kinds of organic pollutants [27]. Considering the respective advantages of graphene and Bi doping, it could be speculated that combined effects would be effective to attain the highest photocatalytic activity under visible light illumination. However, to the best of our knowledge, it has not yet been reported in the literature, i.e. the combined effect of graphene and Bi for the photocatalytic decomposition of MB and herbicide derivative.

In the present work, combining the doping effect, nanostructures and graphene, we design an efficient photocatalyst comprising Bi-TiO<sub>2</sub> nanotube grown on reduced graphene oxide sheets through a facile alkaline hydrothermal approach. The notable aspect of our approach is the simultaneous reduction of GO to graphene and incorporation of Bi into TiO<sub>2</sub>NT. The prepared composites are characterized and their photocatalytic activities are evaluated by studying the decomposition of organic pollutants (Dinoseb and MB) under visible light irradiation.

## 2. Experimental details

### 2.1. Reagents and chemicals

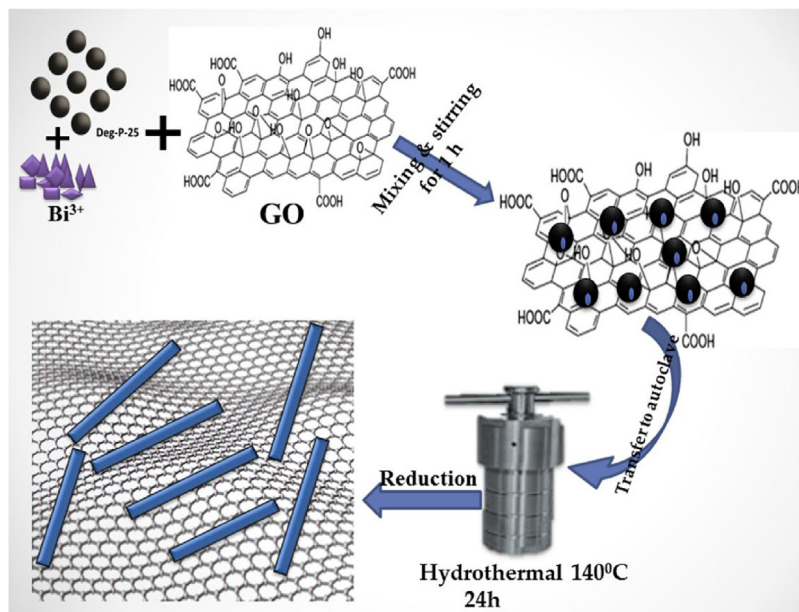
All the chemicals were of analytical grade and were used without further purification. Bismuth nitrate [Bi(NO<sub>3</sub>)<sub>3</sub>·5H<sub>2</sub>O] was purchased from central drug house (CDH) and commercially available TiO<sub>2</sub> nanoparticles (Degussa P25) was a gift sample from Evonik-Degussa, Germany. The model pollutants such as Dinoseb and methylene blue (MB) used for the degradation studies were obtained from Sigma-Aldrich. The other reagent grade chemicals used in this study, such as sodium hydroxide, sulphuric acid, sodium nitrate, potassium permanganate, hydrogen chloride, terephthalic acid (TA), isopropyl alcohol (IPA), benzoquinone, and ethylenediaminetetraacetate (EDTA-2 Na) were obtained from Merck.

### 2.2. Preparation of samples

A series of bismuth doped TiO<sub>2</sub> nanotube graphene (Bi-TNTG) composites with different contents of bismuth (1–4 wt% with respect to Ti) were prepared by a facile alkaline hydrothermal approach initially developed by Kagusa [52]. Graphene oxide (GO) was synthesized from commercially available graphite powder using a modified Hummer's method [53]. A flow chart showing the method involved in the preparation of Bi-doped TiO<sub>2</sub> NT/graphene composites is illustrated in Scheme 1. In a typical process, desired amount (2 wt%) of synthesized GO was suspended into 30 mL of double distilled water and sonicated for 90 min to which 1 g of Degussa P25 was added. A separately dissolved various amount of bismuth nitrate in water was added into above solution and stirred for 1 h to obtain a homogenous suspension. In order to make the above solution concentration up to 10 M, required amount of NaOH was added with vigorous stirring. After 1 h of stirring, the complete mixture was transferred into a Teflon-lined autoclave and heated at 140 °C for 24 h and then cooled down to room temperature. The final grayish color product was filtered and washed with double distilled water followed by acid washing with 0.1 M of HCl, which was then dried at 80 °C for 16 h. Subsequently, the obtained product was rinsed multiple times with double distilled water and then the product was allowed to dry overnight at 80 °C and then ground to obtain a fine powder. It was further subjected to annealing process at 350 °C for 6 h. The final Bi-doped TiO<sub>2</sub> NT/graphene composites were denoted as x-BTNTG, where x stands for 0, 1, 2, 3, 4 wt% of Bi. Single Bi-doped TiO<sub>2</sub> NT and bare TiO<sub>2</sub> NT were also prepared by the similar procedure, but not including the amount of Bi and/or GO.

### 2.3. Materials characterization

X-ray powder diffraction patterns of prepared samples were obtained using Shimadzu XRD (model 6100) with (Cu Kα radiation (1.54065 Å)) operated at a voltage of 30 kV and current of 15 mA. Fourier Transform Infrared spectra were acquired in the range of 400–4000 cm<sup>-1</sup> using a Perkin Elmer spectrum-2. Scanning electron microscopy and energy dispersive spectra were obtained using JEOL-JEM with an accelerating voltage of 20 kV. Transmission electron microscopy (TEM) images of the catalyst were obtained by using a JEOL-JEM 2100 microscope at an accelerating voltage of 120 kV. The optical properties of the samples were determined by UV-vis diffuse reflectance spectra (DRS) using Perkin Elmer Lambda 35 UV-vis spectrophotometer. The spectra were acquired at 300–800 nm using BaSO<sub>4</sub> as a reflectance reference. Electron paramagnetic resonance (EPR) spectra were recorded at 100 K using JEOL-JES-FA200 ESR spectrometer. Brunauer Emmett-Teller specific surface areas (S<sub>BET</sub>) of the photocatalysts were determined



**Scheme 1.** Schematic illustration for the synthesis procedure and structure of Bi-TiO<sub>2</sub> NT/graphene composites.

using model micromeritics flow sorb II (2300). Total organic carbon (TOC) of the sample solution of MB was detected with a Shimadzu TOC analyzer (TOC-V CSH). Photoluminescence spectra (PL) of the samples were recorded at room temperature using Hitachi (F-2500) in reflection mode and an excitation wavelength of 325 nm.

#### 2.4. Catalyst activity and endurance

The photocatalytic activities of the prepared samples were systematically assessed by studying the decomposition of Dinoseb and MB in aqueous solutions under visible light irradiation using commercially available 500W (9500 lumens) linear halogen lamp as a light source, which was vertically placed in an immersion well photochemical reactor. During the photochemical reaction, the photoreactor was circulated with cold water to maintain the ambient reaction temperature. The procedures involved in the preparation of the aqueous solution of organic pollutants and their degradation determination were adopted from our previous work [54]. In a representative procedure, 50 mg of catalyst was mixed with 180 mL of aqueous solution containing the above-mentioned model pollutants with the concentration of 10 mg/L in a photochemical reactor. Before light irradiation, the solution was ultrasonicated for 2 min followed by magnetic stirring for 0.5 h in order to establish the baseline correction after adsorption of organic pollutants on the surface of the catalyst. At certain time interval, 5 mL of aliquots were collected, centrifuged at 6000 rpm, and subsequently filtered to remove the catalyst before analysis. The degradation was monitored by measuring the change in absorbance as a function of time of irradiation of an aqueous solution to desired pollutants (Dinoseb  $\lambda_{\text{max}}$  376 nm, MB 663 nm) with UV-vis spectrophotometer (Model: Perkin Elmer spectrum-2). The degradation efficiency of the catalyst was evaluated from the following expression.

$$\text{Degradation efficiency} = \frac{(C_0 - C_t)}{C_0} \times 100\% \quad (1)$$

Where  $C_0$  is the concentration of Dinoseb or MB after adsorption-desorption equilibrium achieved prior to irradiation and  $C_t$  is the concentration of the mentioned pollutants at different time intervals after the photocatalytic reaction, respectively. A blank test was also conducted by irradiating the model pollutants in the absence of the catalyst to evaluate the role of catalyst in the degradation

process. A separate test of adsorption study of the four catalysts was also carried out to investigate the role of adsorption on photocatalytic degradation of organic pollutant and its experimental details are given in supplementary information. The change in total organic carbon (TOC) contents was also measured by irradiating an aqueous solution of MB in the presence of synthesized catalyst to determine the extent of mineralization.

In addition, the stability and durability of the synthesized Bi-TiO<sub>2</sub> NT/graphene nanotube composites were examined by irradiating MB with the desired catalyst for five consecutive cycles under visible light irradiation. After each experiment, the photocatalyst was washed thoroughly with double distilled water followed by treatment with acetone to remove the unwanted materials and eventually dried at 90 °C to use for next cycle.

#### 2.5. Determination of reactive species

To ascertain the main reactive species formed during the photocatalytic degradation process, different scavengers such as isopropyl alcohol (IPA), 1,4-benzoquinone (BQ) and disodium ethylenediaminetetraacetate (EDTA-2 Na) have been employed to detect hydroxyl radical ( $\cdot\text{OH}$ ), superoxide radical ( $\text{O}_2^{\cdot-}$ ) and hole ( $\text{h}^+$ ), respectively. For this experiment, 2 mM solution of the above scavengers were introduced into an aqueous solution of the desired pollutant before the addition of photocatalyst powder to check the inhibitory effect of scavengers during the photocatalytic reaction under analogous irradiation experimental condition.

In addition, the generation of hydroxyl radical ( $\cdot\text{OH}$ ) on the surface of the catalyst in photocatalytic process was analyzed by using terephthalic acid (TA) as a probe molecule. It has been well known that the hydroxyl radical ( $\cdot\text{OH}$ ) readily reacts with terephthalic acid to produce highly fluorescent adduct, a 2-hydroxyterephthalic acid which can be monitored by recording the PL signal at 425 nm emission wavelength. The PL intensity is directly related to the concentration of hydroxyl radicals which is formed on the catalyst surface during the course of the reaction. The experimental condition is relatively similar as performed during the measurement of photocatalytic activity catalyst, but replacing the aqueous solution of organic pollutants by TA ( $5 \times 10^{-4}$  M) in dilute sodium hydroxide solution. After irradiation with visible light at different times, the

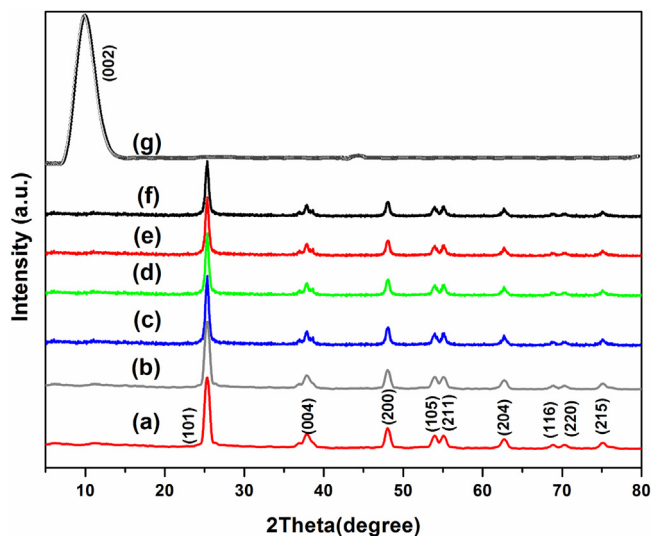


**Fig. 1.** XRD patterns of (a) TNT, (b) 2-BTNT, (c) TNTG, (d-f) 1–3%-BTNTG, and (g) GO.

samples were withdrawn, centrifuged, and then the supernatant solution was analyzed to quantify the product using Hitachi F-2500 spectrometer with the excitation wavelength fixed at 310 nm.

### 3. Results and discussion

In order to make use of full range of the visible region of the electromagnetic spectrum, Bi-doped TiO<sub>2</sub> nanotube graphene composite was prepared by a facile and green hydrothermal approach. During this process, GO was transformed into graphene sheet and simultaneously Bi was embedded into the TiO<sub>2</sub> lattice. Meanwhile, the structure of TiO<sub>2</sub> was transformed from nanoparticles to nanotubes in the same treatment. The process for the preparation of Bi-TiO<sub>2</sub> nanotube/graphene composite is illustrated in **Scheme 1**. The prepared catalyst was characterized by different standard techniques to clarify the nature of graphene and also to determine the morphology and phase characteristics of the synthesized materials. The photocatalytic performances of prepared catalysts were evaluated by studying the decomposition of Dinoeb and MB under visible light irradiation. Furthermore, to confirm the sole contribution of hydroxyl radical which plays the decisive role in the photocatalytic degradation reaction was investigated by quenching and terephthalic acid measurements.

#### 3.1. XRD analysis

XRD analysis was employed to analyze the crystal phase and structure of the prepared different samples as illustrated in **Fig. 1**. It could be seen from the figure that all diffraction peaks of bare TiO<sub>2</sub> NT (TNT), 2 wt% of Bi-doped TiO<sub>2</sub> NT (2-BTNT), TiO<sub>2</sub> NT/graphene (TNTG) and different wt% of Bi-doped TiO<sub>2</sub> NT/graphene (1,2,3-BTNTG) composites are observed at 2θ values of 25.3°, 37.9°, 48.0°, 54.0°, 55.2°, 62.7°, 68.9°, 70.4°, and 75.2° respectively. All the peaks observed in the XRD pattern can be well indexed to the anatase crystal phase as shown in (**Fig. 1(a-f)**), [23]. The results indicate that all the samples are in anatase phase without any ambiguity, declaring the purity of the samples and no obvious characteristics peaks regarding the brookite or rutile phases as well as phases induced by the dopants were observed in anyone of the samples. On the basis of results, it might have assumed that bismuth and graphene are completely incorporated into TiO<sub>2</sub> NT and have no obvious influence on the crystal phase of TiO<sub>2</sub>. As viewed from **Fig. 1g**, there is an obvious diffraction peak at 10.3° corresponding to the (002) reflection of GO, which indicates that graphite was completely oxidized

**Table 1**  
Physicochemical properties of xBi-TNTG (x = 1,2,3,4 wt%) composites.

Sample	Crystallite size (nm)	S <sub>BET</sub> (m <sup>2</sup> g <sup>-1</sup> )	Optical bandgap (eV)
TNT	16.43	74.23	3.12
TNTG	12.87	96.74	2.97
2-BTNT	14.32	79.61	2.93
1-BTNTG	11.29	130.94	2.83
2-BTNTG	10.45	158.80	2.78
3-BTNTG	12.21	124.12	2.75
4-BTNTG	12.76	103.25	2.73

into GO sheets [23,55]. From **Fig. 1(b-f)**, it could be noticed that no characteristic peak of GO is observed in the corresponding composites, which could be attributed to the complete conversion of GO to reduce graphene after hydrothermal process implying the reduction efficiency of the provided basic medium. The other reason for the non-appearance of the typical diffraction peak of graphene in the final composites could be due to the fact that the anatase main peak located at 25.4° shadowed the characteristic peak of graphene, which is in good agreement with previous findings [23,55]. The average crystallite sizes of the prepared samples were determined by using Scherrer equation based on the XRD peak broadening of the (101) peak. As mentioned in **Table 1**, the composites material displayed the crystallite sizes in the range of 10–13 nm, which is smaller than that of the pure TiO<sub>2</sub> (16.4 nm) nanotube.

#### 3.2. FTIR analysis

FTIR spectra were carried out to understand the nature of graphene as well as its interaction with TiO<sub>2</sub> nanotube besides bismuth. **Fig. 2** displays the FT-IR spectra of GO, TiO<sub>2</sub>NT, (TNT) TiO<sub>2</sub>NT/graphene (TNTG) composite and Bi-TiO<sub>2</sub>NT/graphene (2-BTNTG) composite. The broad peaks appeared at about 3428 cm<sup>-1</sup> and 1352 cm<sup>-1</sup> in the spectrum of TNTG, and 2-BTNTG composites could be attributed to the surface bound O-H group and tertiary C-OH, respectively [56]. Additionally, the peak appeared at around 1584 cm<sup>-1</sup> in the same composite materials is ascribed to the skeletal vibration of graphene [57]. The FTIR spectrum of GO shows the typical characteristic peaks of oxygen-containing functional groups such as, carbonyl (1720 cm<sup>-1</sup>), alkoxy & epoxy (1038 and 1242 cm<sup>-1</sup>), which proves that the graphite was completely oxidized into GO. The intensity of all oxygen functional group peaks was found to decrease in the composite materials on

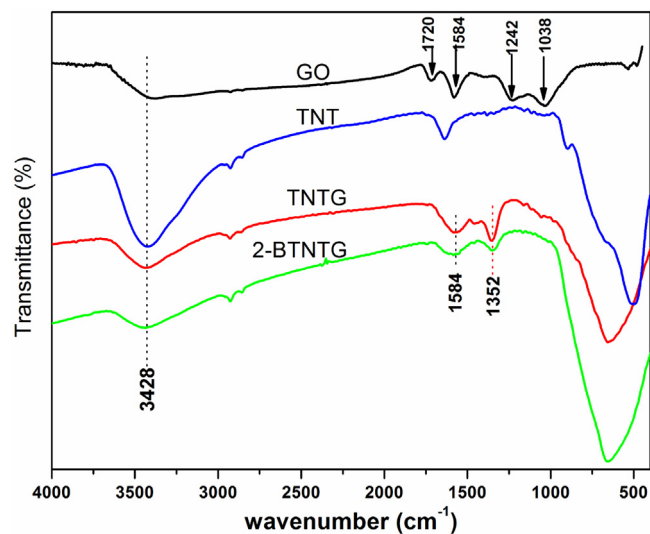


**Fig. 2.** FT-IR spectra of GO, TNT, TNTG and 2-BTNTG.

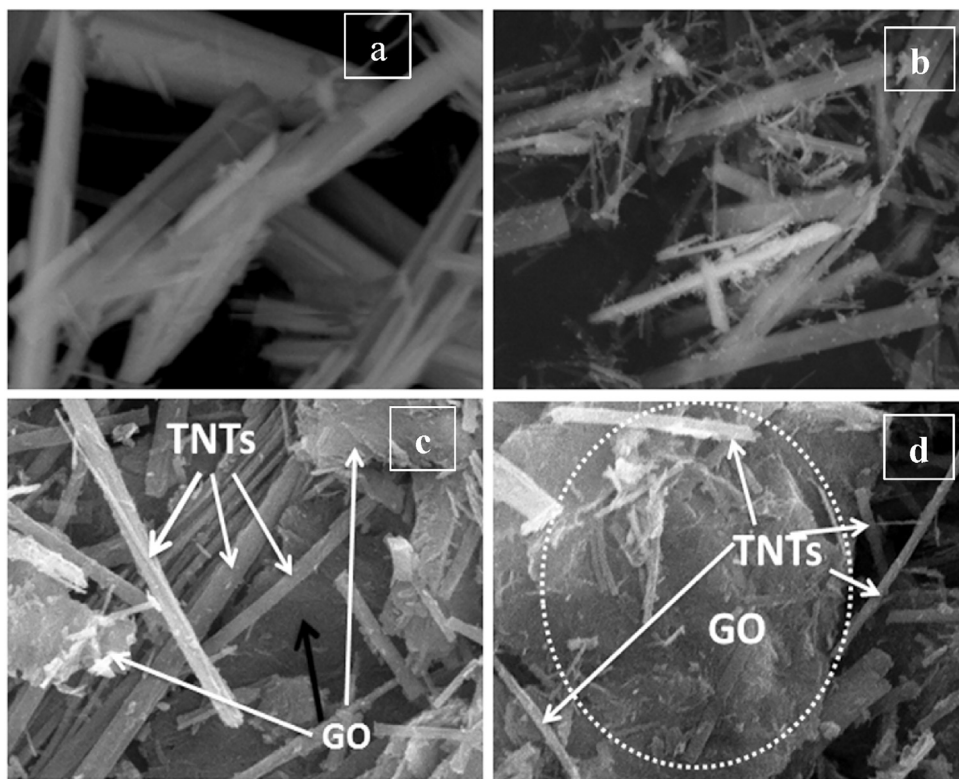


**Fig. 3.** SEM images of TNT (a), 2-BTNT (b), 2-BTNTG (c,d).

hydrothermal treatment [23,55], indicating successful conversion of GO to a reduced form of graphene. These results coincide with XRD results where the main peak at 10.3° disappeared after hydrothermal treatment in all composite materials, suggesting the significant reduction of GO. For pure TNT, the peak at around 1634 cm<sup>-1</sup> is ascribed to the bending vibration of physically adsorbed water molecule [27]. In addition, Pure TiO<sub>2</sub> NT(TNT) displayed a low frequency sharp peak around 508 cm<sup>-1</sup>, could be attributed to the stretching vibration of Ti—O—Ti bonds [55]. However, in the composites of graphene and TiO<sub>2</sub>NTs such as TNTG and 2-BTNTG composites, the broad absorption below 1000 cm<sup>-1</sup> was much broader than the pure TiO<sub>2</sub> NT and slightly shifted toward higher wavenumber [23,57]. This might be due to the combined interaction of Ti—O—Ti, Ti—O—C or Ti—O—Bi vibrations. The presence of above chemically interacted bonds in the composite materials confirmed the reduction of GO to graphene as well as simultaneous incorporation of graphene with bismuth in TiO<sub>2</sub>NT.

### 3.3. Microstructure and BET surface area analysis

The surface morphology of bare TNT, 2-BTNT and 2-BTNTG composite was examined using SEM as shown in Fig. 3. The SEM image of bare TiO<sub>2</sub> NTs demonstrated in Fig. 3a clearly indicates that TiO<sub>2</sub> NT consists of tubular structure as reported earlier [25]. Fig. 3b clearly indicates the dispersion of Bi ion on the surface of TiO<sub>2</sub> NT, evidencing the bismuth doping into TNT. It could be seen from the SEM images of 2-BTNTG (Fig. 3c, d) that the several nanotubes of 2 wt% of Bi-doped TiO<sub>2</sub> anchored on the surface of graphene, implying the interconnection network between Bi-TNT and graphene. To get more details about the intimate contact between TNT and graphene, we have carried out TEM analysis of 2-BTNTG, as shown in Fig. 4. It is clear from both the Fig. 4a & b that graphene sheets are well decorated by the Bi-TNTs, resulting good attachment of Bi-TNTs in the composites. This intimate contact between TNT and graphene evidenced by SEM and TEM images would play the role

of interfacial charge transfer upon irradiation and could be responsible for enhanced photocatalytic activity. In order to unveil the presence of Ti, O, C and Bi, elemental analysis of 2-BTNTG composite was carried out as demonstrated by energy dispersive spectra (EDS) analysis as shown in Fig. 1S. The presence of C and Bi ensure that the both species are successfully incorporated into TNT. The existence of C also suggests that TiO<sub>2</sub> nanotubes are anchored on the graphene surfaces. These results are in good agreement with XRD and FT-IR, where graphene interaction with TNT has been elaborated.

The specific surface areas of pure TiO<sub>2</sub> NT and Bi-TiO<sub>2</sub> NT/graphene composites with different wt% of bismuth were determined by N<sub>2</sub> gas adsorption measurement. The BET surface area of doped, undoped, and composite materials are summarized in Table 1. It could be seen from the table values that the specific surface area of all the composite materials are comparatively higher than that of the undoped and Bi-TiO<sub>2</sub> NT. This could be attributed to the existence of graphene sheet in the resulting materials, which has the high theoretical surface area value as 2600 m<sup>2</sup>/g [58]. On the basis of the analysis, it was observed that the surface areas of the Bi-TiO<sub>2</sub> NT/graphene composites increases up to a certain limit i.e. 2 wt% and then decreases with the increase in bismuth content into TiO<sub>2</sub> NT/graphene. This might be due to the agglomeration of NT, resulting in low surface area of the higher doping contents composites. This high surface area may play an important role in the enhancement of the photocatalytic activity of the synthesized materials.

### 3.4. Photoluminescence (PL) and EPR spectra analysis

The photocatalytic activity of a catalyst is not only determined by the light absorption intensity/visible range but also by the photogenerated electron-hole separation. PL analysis of bare TiO<sub>2</sub> NT, Bi-TiO<sub>2</sub> NT and 1, 2, 3, & 4 wt% Bi-TiO<sub>2</sub> NT/graphene composites were carried out by exciting the above materials at 325 nm and

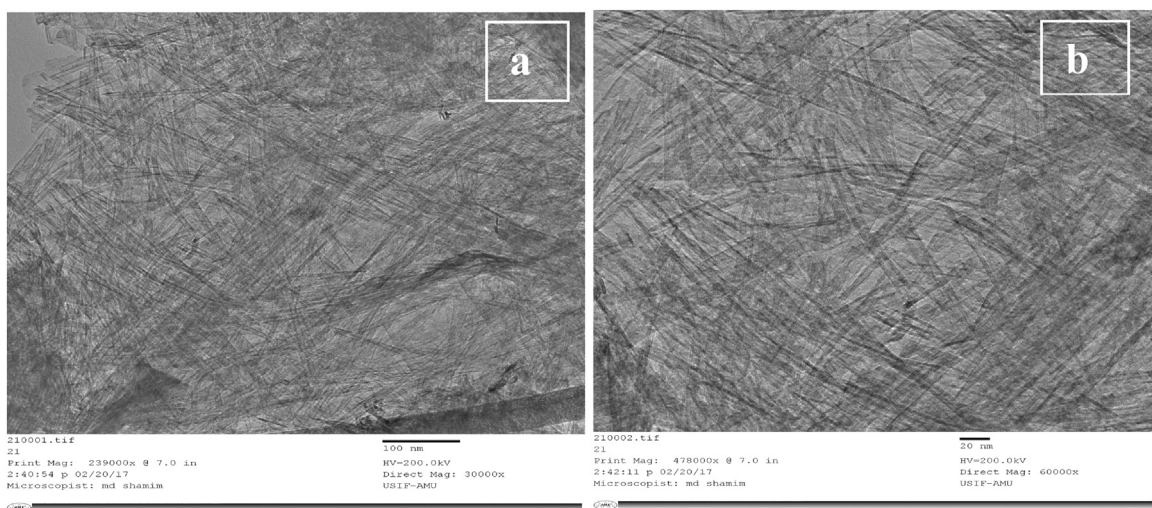


**Fig. 4.** TEM images of 2-BTNTG, (a) at low and (b) at high resolution.

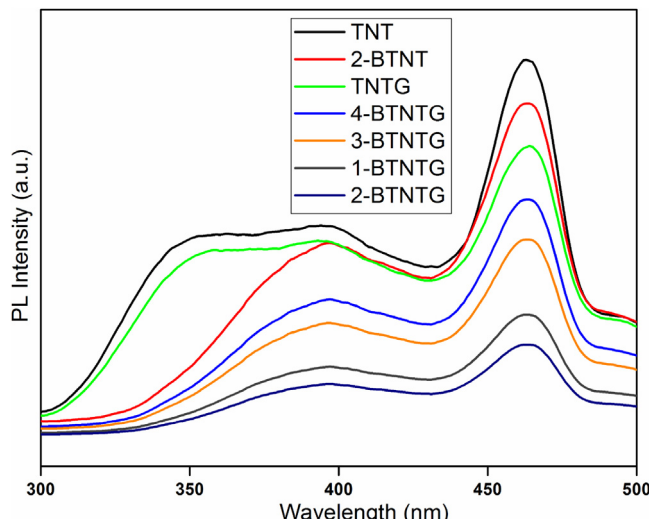


**Fig. 5.** PL emission spectra of TNT, 2-BTNT, TNTG, 1-BTNTG, 2-BTNTG, 3-BTNTG and 4-BTNTG at excitation wavelength of 325 nm.

The emission spectra were recorded as shown in Fig. 5. It is well known that the PL intensity is directly related to the recombination of charge carriers. The higher the PL intensity, higher would be the recombination rate of photogenerated charge carriers [25]. It could be seen from the figure that all the graphene-containing catalysts show less intense peaks as compared to their counterparts bismuth doped and undoped TiO<sub>2</sub> NT. Interestingly, the emission peak of TiO<sub>2</sub> NT/graphene was substantially quenched in intensity as compared to that of bismuth doped TiO<sub>2</sub> NT. The result suggests that the photogenerated electron-hole pair was significantly diminished by the generated interface between TiO<sub>2</sub> NT and graphene owing to its ability to transport the electron and minimize the recombination of charge carriers [27]. Compared to all samples, the PL intensity of Bi-TiO<sub>2</sub> NT/graphene composites was decreased effectively, indicating that bismuth also plays a leading role in diminishing of charge carriers [59]. This could be due to the formation of impurity level by doped Bi ions between the VB and CB of TiO<sub>2</sub> NT. The excited electron firstly moves to the internal band of catalyst formed by Bi<sup>3+</sup> species and then goes to the CB of TiO<sub>2</sub> NT [27], which may in turn transfers to the empty electronic states of graphene sheet through interfacial charge transfer process resulting in the reduction of PL intensity [23]. In addition, the PL intensity was found to increase

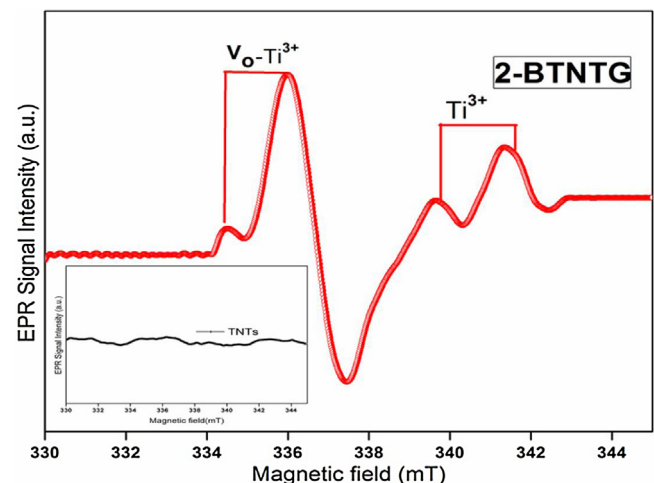


**Fig. 6.** EPR signals of 2-BTNTG and pure TNT (inset).

with an increase in doping content of bismuth in the sequence: 2 wt% < 1 wt% < 3 wt% < 4 wt%, indicating that least recombination rate of electron hole pair takes place in the case of 2-BTNTG. The PL results reveal that the combined effect of bismuth and graphene effectively retard the recombination of charge carriers, leading the enhanced photocatalytic activity of composite materials.

To unveil the existence of Ti<sup>3+</sup> into composite material, low-temperature electron paramagnetic resonance (EPR) was performed. The EPR spectra for undoped TNT and 2 wt% Bi-doped TiO<sub>2</sub>NTs/graphene (2-BTNTG) were recorded and the results are shown in Fig. 6. It is well known that EPR is insensitive to Ti<sup>4+</sup> (d<sup>0</sup>) electron species, and thus no EPR signal was observed in the case of undoped TiO<sub>2</sub> NTs as shown in the inset of the figure. It is obvious from the figure that 2-BTNTG shows unambiguously two strong EPR signals at about g = 1.983 and 2.002, which could be ascribed to the presence of Ti<sup>3+</sup> and oxygen vacancies, respectively. These results are in good agreement with the previous study, where authors have reported that the oxygen vacancy has a g-value of 2.004 and paramagnetic Ti<sup>3+</sup> at 1.94–1.99 [60]. The reason behind the creation of Ti<sup>3+</sup> into TiO<sub>2</sub> is due to the formation of cross-linked bond–Ti<sup>4+</sup>–O–Bi<sup>3+</sup>, which is coexisted with oxygen vacancies [28]. The existence of –Ti–O–Bi– bond was confirmed previously by Raman analysis [61]. The potential advantage of Ti<sup>3+</sup> and oxygen vacancies is that they can provide the trapping cen-

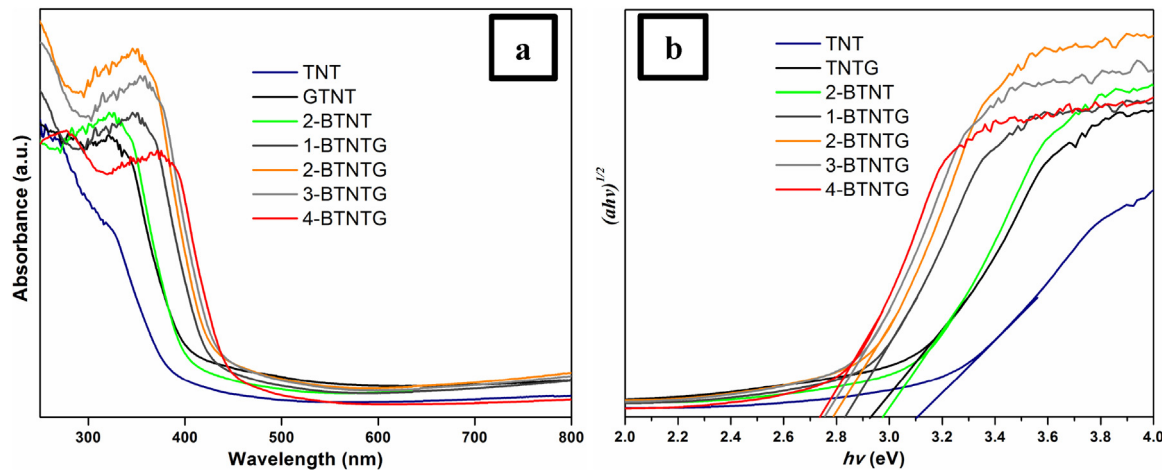


**Fig. 7.** (a) UV-vis diffuse reflectance spectra of different samples, and (b) their corresponding Tauc's plot.

ter for photogenerated charge carriers which may in turn reduce the recombination of photogenerated electron hole pair, thereby enhancing the photocatalytic activity.

### 3.5. UV-vis DRS analysis

The optical response of the prepared pure  $\text{TiO}_2$  NT,  $\text{TiO}_2$ /graphene composite and different doping contents of bismuth onto  $\text{TiO}_2$  NT/graphene composites was investigated using UV-vis diffuse reflectance analysis and the results are shown in Fig. 7. From the figure it could be observed that graphene incorporated  $\text{TiO}_2$  NT showed little enhancement of its absorbance towards visible region as compared to bare  $\text{TiO}_2$  NT. Moreover, an obvious enhancement in the visible region could be seen for Bi- $\text{TiO}_2$  NT, and Bi- $\text{TiO}_2$  NT/graphene composites as compared to pure  $\text{TiO}_2$  NT, implying that bismuth and graphene are successfully incorporated into the lattice of  $\text{TiO}_2$  NT. The doping of bismuth leads to the formation of an impurity level between the top of the (lone pair)  $\text{Bi}^{3+}$  6 s band and the bottom of the  $\text{Ti}^{4+}$  3d band [27,28,61]. It is worth noting that the threshold wavelength increases with the increase of bismuth content into  $\text{TiO}_2$  NT/graphene composites, which leads to decrease the bandgap energy. The bandgap energies of Bi- $\text{TiO}_2$ ,  $\text{TiO}_2$  NT/graphene and different wt% Bi- $\text{TiO}_2$  NT/graphene were estimated by the Tauc plot equation (2) as shown below.

$$[ahv] = A(hv-Eg)^n/2 \quad (2)$$

Where  $Eg$  is the band gap of the proposed semiconductor (eV),  $h$  is Planck's constant,  $c$  is the speed of light,  $\nu$  is the frequency of light,  $A$  is the absorption constant and  $a$  is the absorption coefficient.  $n$  is 1 and 4 for direct and indirect bandgap semiconducting materials, respectively. A plot of  $(ahv)^{1/2}$  vs photon energy  $h\nu$  can be obtained by using the value of y axis ( $(ahv)^{1/2}=0$ ) is zero. The resulting plot indicates that the bandgap energies of the as-prepared samples were estimated to be in the range of 3.17–2.73 eV as shown in Fig. 7b and Table 1. These results are in good agreement with the qualitative observation of the red shift illustrated in Fig. 7a. The results clearly demonstrate that the simultaneous incorporation of bismuth and graphene into  $\text{TiO}_2$  NT markedly shifts the absorption towards visible region.

### 3.6. Adsorption measurement

To investigate the adsorption of MB and dinoseb under dark onto the synthesized catalysts (TNT, TNTG, 2-BTNT and 2-BTNTG), a separate dark adsorption experiment was carried out by stirring an aqueous suspension of pollutants at room temperature for 12 h. It

is well known that in heterogeneous photocatalysis better adsorption of the pollutants onto the catalysts led to high degradation rate [62,63]. Fig. 2S shows the percent adsorption of MB and dinoseb in the presence of different photocatalysts under dark. It could be seen from the figure that 2-BTNTG shows better adsorbability followed by TNTG, 2-BTNT and TNT in an aqueous suspension of both pollutants. The better adsorption of MB onto the surface of 2-BTNTG may be attributed to the combined effect of Bi and graphene that provides high surface area and facilitates to transfer organic pollutants from solution to the interface which subsequently decomposed the organic pollutants. It is clear from the figure that the Bi also promotes the adsorption of organic pollutants onto the surface of  $\text{TiO}_2$  nanotube and this could be ascribed to its unique structure and the high surface area which provides more active sites for the adsorption of organic pollutants compared to the pure  $\text{TiO}_2$  nanotube. The adsorption results are in agreement with the order of surface area of the catalysts. Compared to dinoseb, MB showed better adsorption in all samples and more profound adsorption was observed in the case of graphene-based catalysts. The reason for the enhanced adsorptivity of graphene-based catalysts is due to  $\pi$ - $\pi$  stacking between aromatic regions of graphene and MB, which has benzene rings in its molecular structure facilitating the  $\pi$ - $\pi$  conjugation with graphene. It is clear from the figure that MB is better adsorbed on the surface of 2-BTNTG compared to dinoseb and the reason for the better adsorption of MB on catalysts surface is that MB has more benzene rings compared to latter one.

### 3.7. Photocatalytic activity and endurance

The potential application of the prepared composites was evaluated by studying the degradation of Dinoseb (herbicide derivative) and MB (textile dye) under visible light source. Dinoseb is a well-known phenolic herbicide, highly toxic by ingestion and skin exposure, which is usually used for the selective control of grass and broadleaf weeds and was found to be most persistent contaminants [64]. In most the circumstances, the reported half-life of dinoseb was ranged from 5 to 31 days, therefore, its removal was found to be very difficult [65,66]. The photocatalytic degradation of an aqueous suspension of dinoseb in the presence of different catalysts was estimated by studying the change in absorbance ( $\lambda_{\text{max}} = 376$  nm) as a function of irradiation time under visible light source. Fig. 8a shows the change in absorption intensity of dinoseb as a function time in the presence of 2-BTNTG whereas 8 b shows the change in concentration of dinoseb as a function of time in the presence of different catalysts. It is well known that the adsorption of organic pollutants on catalyst surface plays an important

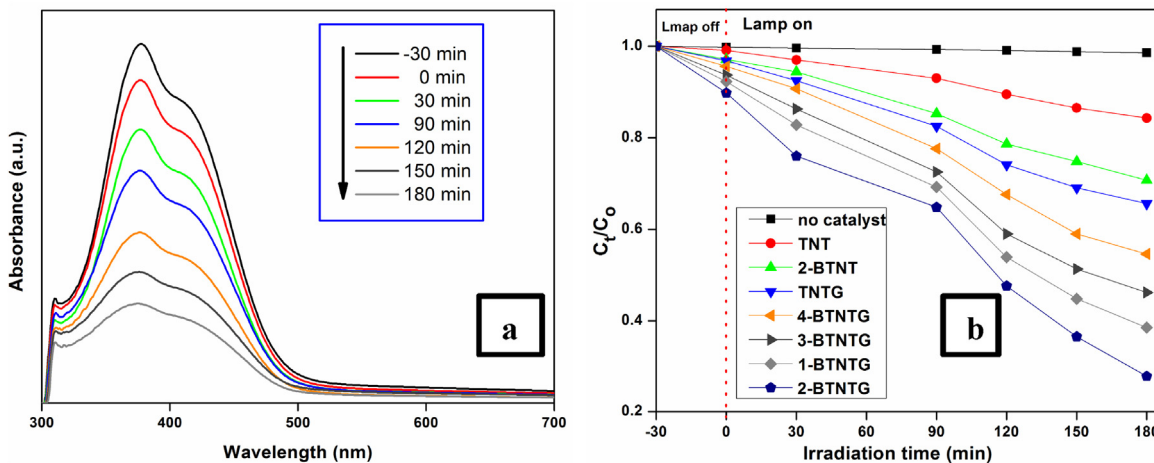


**Fig. 8.** (a) change in the absorption intensity as a function of time on irradiation of an aqueous solution of dinoseb in the presence of 2-BTNTG under visible light and (b) change in the concentration of dinoseb as a function of time in the presence of different samples under visible light source.

role in the photocatalytic degradation of organic pollutants [46]. Before light illumination, all experiments were performed in the dark for 30 min to achieve the adsorption-desorption equilibrium. In addition, a blank experiment under visible light (in the absence of catalyst) was also conducted to determine the role of catalyst. Fig. 8a shows that 72% degradation of dinoseb takes place in 180 min of light illumination. On the other hand Fig. 8b shows that the photocatalytic efficiency of the synthesized catalysts for degradation of dinoseb increases in the order TNT < 2-BTNT < TNTG 4-BTNTG < 3-BTNTG < 1-BTNTG < 2-BTNTG. It is interesting to note that the highest efficiency was observed in the case of 2-BTNTG, which could be attributed to the high surface area leading to more adsorption and hence showing the highest photocatalytic activity. This remarkable enhancement in photocatalytic activity is mainly due to the contribution of graphene, which forms an intimate contact between Bi-TiO<sub>2</sub> NT and graphene resulting in efficient separation of charge carriers [67]. In addition, it is also observed from the figure that the photocatalytic activity increases with increasing the doping content of Bi from 1 wt% to 2 wt% in TiO<sub>2</sub> NT/graphene composite. Further increase in Bi doping content led to curtail the photocatalytic activity. The reason for inferior photocatalytic activity of high doping content of bismuth (>2 wt%) in TiO<sub>2</sub> NTs/graphene composites is the greater expansion of threshold wavelength to the visible region resulting to more decrease

in bandgap energy, consequently hindering the separation rate of charge carriers as evidenced by the PL result. The deterioration in photocatalytic activity after optimum doping content might also be due to the lower dispersion or serious segregation of Bi on the TiO<sub>2</sub> NT surface [68].

Additionally, the photocatalytic activity of the prepared composites is further tested by studying the degradation of MB under the analogous conditions as applied in the previous pollutant degradation. The absorption intensity of MB centered at 663 nm gradually decreases with increase in irradiation time for 2-BTNTG composite and 95% of degradation was observed during 60 min of irradiation as depicted in Fig. 9a. Fig. 9b shows the change in concentration of MB as a function of irradiation time in the presence of different samples. The degradation trends follow the same patterns as observed in the case of dinoseb and once again the highest activity was observed with 2-BTNTG for the degradation of MB also. The pure TiO<sub>2</sub> NT and TiO<sub>2</sub> NT/graphene composite Exhibit 57 and 68% of degradation under visible light due to the self-sensitized mechanism. Under visible light illumination, an electron can excite from HOMO to LUMO level of MB which may in turn get transferred to the CB of TiO<sub>2</sub> NTs and subsequently participate in degradation reaction after converting into reactive oxygen species (ROS).

In addition, the mineralization of MB was also evaluated by studying the depletion in TOC content as a function of time on irra-

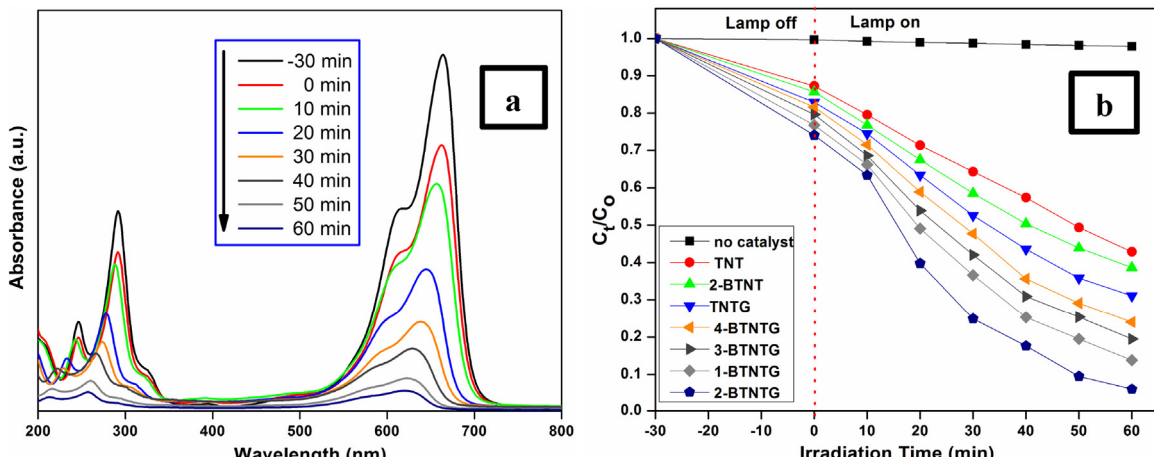


**Fig. 9.** (a) change in the absorption intensity of MB as a function of time on irradiation of an aqueous solution of MB in the presence of 2-BTNTG under visible light, (b) change in the concentration of MB as a function of irradiation time in the presence of different samples under visible light source.

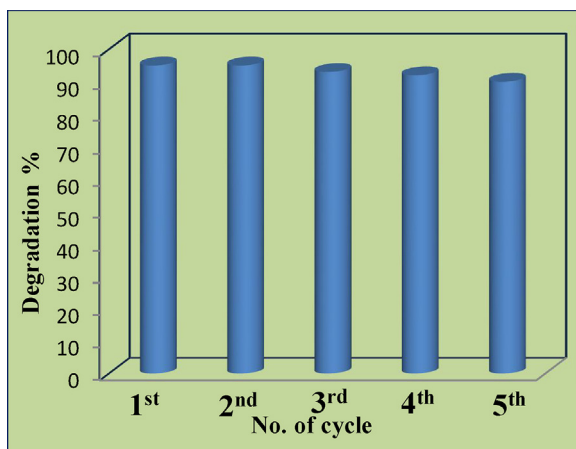


**Fig. 10.** percent degradation of MB over 2-BTNTG under visible light irradiation for different run cycles.

diation of an aqueous solution of MB in the presence of a most active catalyst (2-BTNTG). The total organic carbon (TOC) removal curve is illustrated in Fig. 3S, depicting the mineralization of MB. From the result it could be seen that 48% of mineralization takes place after 180 min of light illumination, manifesting the strong photocatalytic ability of 2-BTNTG.

Besides activity, the stability of photocatalyst is also an important factor for its assessment and practical application. Therefore, to investigate the reusability of the prepared 2-BTNTG, the degradation of MB was monitored for five run cycles. After each experiment, which was conducted for 60 min of photodegradation, the separated photocatalyst was washed thoroughly with acetone followed by double distilled water and then dried at 90 °C for 4 h and then used for next cycle. Fig. 10 shows the percent degradation of MB for five successive runs in the presence of 2-BTNTG under visible light source. It could be seen from Fig. 10 that after five successive runs, the photocatalytic degradation efficiency of the catalyst remains more or less same within the experimental error limits.

### 3.8. Determination of reactive species and photocatalytic mechanism

In order to get insight into the photocatalytic mechanism, trapping experiments were conducted to ascertain the leading role of reactive species in photocatalysis. Different scavengers such as, disodium ethylenediaminetetraacetate (EDTA-2 Na) (as a quencher of hole), isopropyl alcohol (IPA) (as a quencher of HO•) and benzoquinone (BQ) (as a quencher of O<sub>2</sub><sup>-</sup>) were respectively introduced just before the addition of catalyst in aqueous solution of MB as discussed in previous literature [54]. As shown in Fig. 11, no inhibitory effects were observed after the addition of BQ and disodium ethylenediaminetetraacetate (EDTA-2 Na) into the reaction medium. The results indicate that the hole and superoxide do not impart contribution in photocatalytic degradation of MB. Meanwhile, IPA leads to a significant reduction in photocatalytic degradation of MB, implying the involvement of HO• being the major species in the photocatalytic degradation process.

To further investigate the role of HO• radical, which mainly conduce to the degradation of MB and dinoseb over 2-BTNTG under visible light irradiation, quantification experiment of HO• radicals formation was conducted by a photoluminescence (PL) technique using terephthalic acid (TA) as a probe molecule. It could be seen from Fig. 12 that the PL intensity at 425 nm increases with the increase of irradiation time, evidencing the generation of hydroxyl radicals. In general, PL intensity is mainly originated due to the chemical reaction between terephthalic acid and HO• formed at the

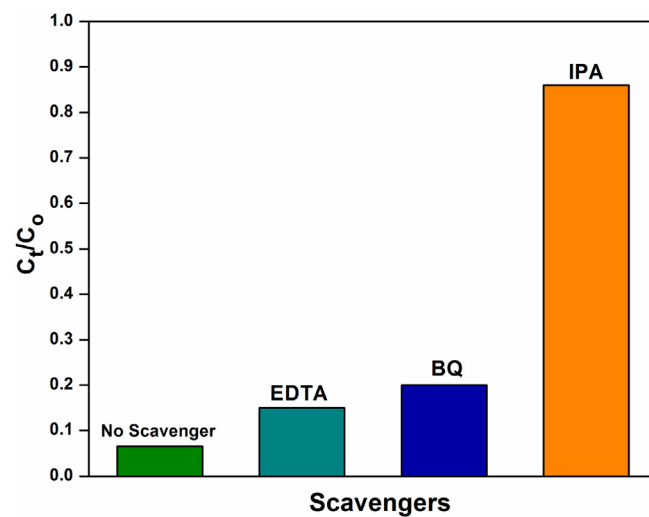


**Fig. 11.** Effect of reactive species on the photocatalytic degradation of MB over 2-BTNTG.

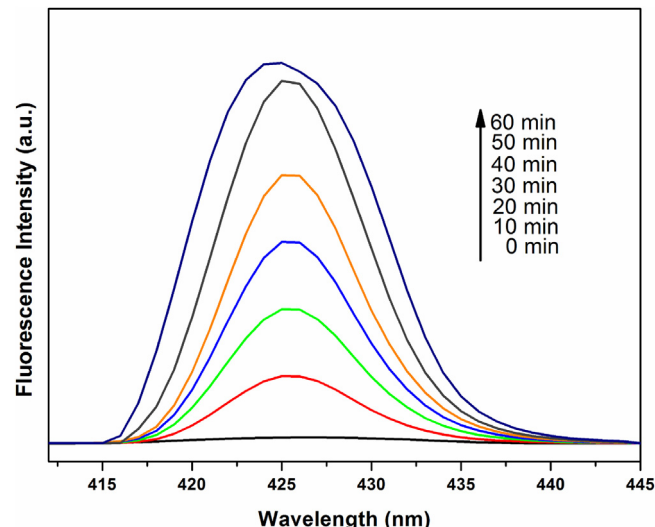


**Fig. 12.** Generation of HO• radicals in 2-BTNTG suspension measured by fluorescence method with terephthalic acid.

2-BTNTG/water interface via photocatalytic reactions [69]. However, a straight line was observed under dark condition, which could easily be understood that no HO• was generated under dark condition. The presence of HO• radicals in the photocatalytic process of 2-BTNTG could be well explained by the transfer mechanism when the electron excited from VB to CB subsequently transferred to the Fermi level of graphene because graphene is known to have lower Fermi level than TiO<sub>2</sub> and energetically is favorable to capture electron [70]. After transferring to graphene level, electrons would subsequently capture by the sorbed species and finally converted into HO• radicals by a well-known mechanism discussed in the previous literature [71]. The whole mechanism involving the generation of reactive oxygen species (ROS) has been discussed below.

Considering the aforementioned results and discussions, a proposed mechanism for the degradation of dinoseb and MB over the most active 2-BTNTG composite is shown in Fig. 13. In general, when a semiconductor absorbs photon of energy equal to or greater than its bandgap, an electron is excited from VB to CB leaving behind an electron vacancy "hole" in the VB which may in turn participate in the redox reaction and degrade the organic pollu-

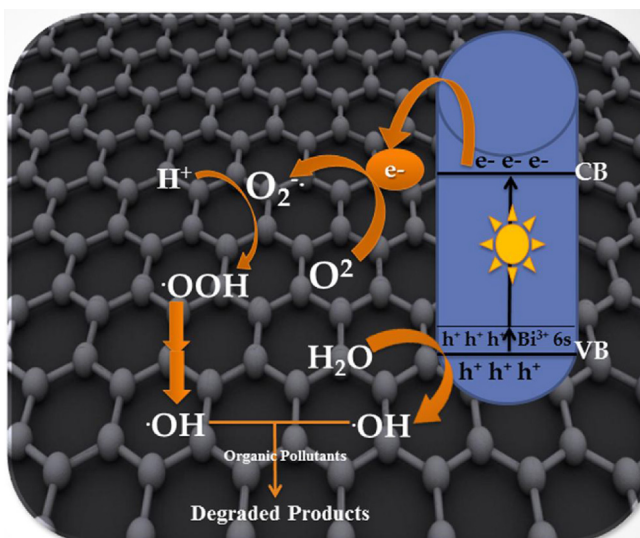
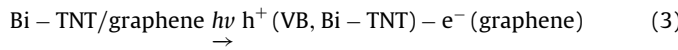


**Fig. 13.** Proposed photocatalytic mechanism of Bi-doped  $\text{TiO}_2$ NTs/graphene composite.

tants. It is well known that Bi introduces energy level below the CB edge of  $\text{TiO}_2$ , resulting in extending the spectral response to the visible region, which plays a significant role in the generation of the electron-hole pair [28]. Upon irradiation of catalyst, the electrons are excited from impurity level of  $\text{TiO}_2$  NT (created by Bi species) to CB of TNT and the simultaneously equal number of holes will be generated in the impurity level. Following this, the photogenerated electrons in the CB of  $\text{TiO}_2$ NT could be effectively transferred to the graphene sheet through a percolation mechanism [72]. When the electron-hole pair separation is maintained, electrons get accumulated on the graphene sheet and holes are accumulated at impurity level. These subsequently captured by the sorbed species to convert into reactive oxygen species (ROS) through different paths as given in Eqs. (3)–(8). The reactive hydroxyl radicals ( $\cdot\text{OH}$ ), which plays the major role in the degradation of MB and dinoseb (as established by quenching studies), could be generated either by the reaction of hole with water or from hydrogen peroxide generated in the reaction mixture [27,73]. The reason for the generation of hydroxyl radicals being the main species instead of superoxide is that the work function of graphene is less negative than the reduction potential of oxygen ( $E_{\text{o}}(\text{O}_2/\cdot\text{O}_2^-) = -0.046 \text{ eV vs SHE}$ ) [70,74]. The hydroxyl radicals generated in the reaction mixture being powerful strong oxidizing agent may play the vital role in the degradation of dinoseb and MB in the presence of photocatalyst. The overall photocatalytic activity could be attributed to the synergistic action of graphene and Bi-TiO<sub>2</sub> NT, which plays an important role in the separation of charge carriers thereby improving the photocatalytic activity. The other reasons for enhanced photocatalytic activity could be ascribed due to the formation of oxygen vacancy,  $\text{Ti}^{3+}$  centers and other defects created on Bi-doping and also incorporation graphene moiety.



#### 4. Conclusions

Bi-doped  $\text{TiO}_2$ NT/graphene composites with different wt% of Bi are prepared by an alkaline hydrothermal method. The method involves the transformation of GO to graphene and simultaneous incorporation of Bi into  $\text{TiO}_2$  NT. The combined effect of Bi and graphene extended the spectral response of  $\text{TiO}_2$  NT to the visible region of the solar spectrum evidenced by the UV-vis absorption spectra. The photocatalytic activity of as-synthesized composites is examined by using dinoseb and MB as probe organic pollutants. The photocatalytic activity results revealed that 2 wt% Bi-doped  $\text{TiO}_2$ NT/graphene is found to be the most active photocatalyst for the degradation of dinoseb and MB under visible light irradiation as compared to their counterparts. The enhanced photocatalytic activity could be attributed to the enhanced light absorption and efficient separation of charge carriers due to graphene and Bi incorporation. Moreover, the underlying mechanism involving photocatalytic degradation of organic pollutants over 2-BTNTG is explored using trapping experiments, suggesting that the degradation solely determines by  $\cdot\text{OH}$  radicals. The reusability tests revealed the strong durability of the catalyst. The mechanism for enhanced photocatalytic activity is proposed with full details. The research work will provide a new path for the green synthesis of metals and carbonaceous materials onto  $\text{TiO}_2$  with controlled morphology and photocatalytic properties.

#### Acknowledgements

This work was financially supported by research project from Ministry of Mines, government of India, New Delhi and Alexander von Humboldt Foundation, Germany under research group linkage program. The authors would also like to acknowledge DST and UGC, for research support (DRS II, PURSE & FIST) to the Department of Chemistry, AMU, Aligarh. We are thankful to Dr. Faryal Idrees for her valuable suggestions in drafting the manuscript.

Experimental details of adsorption study, EDS spectra, a bar graph of adsorption study and figure of change in TOC content of MB.

#### Appendix A. Supplementary data

Supplementary data associated with this article can be found, in the online version, at <http://dx.doi.org/10.1016/j.apcatb.2017.06.016>.

#### References

- [1] Y. Tang, G. Zhang, C. Liu, S. Luo, X. Xu, L. Chen, B. Wang, Magnetic  $\text{TiO}_2$ -graphene composite as a high-performance and recyclable platform for efficient photocatalytic removal of herbicides from water, *J. Hazard. Mater.* 252–253 (252) (2013) 115–122.
- [2] S. Mohammadi, A. Kargari, H. Sanaeepur, K. Abbassian, A. Najafi, E. Mofarrah, Phenol removal from industrial wastewaters: a short review, *Desalin. Water Treat.* 53 (8) (2015) 2215–2234.
- [3] M. Sun, T. Yan, Q. Yan, H. Liu, L. Yan, Y. Zhang, B. Du, Novel visible-light driven  $\text{g-C}_3\text{N}_4/\text{Zn}_{0.25}\text{Cd}_{0.75}\text{S}$  composite photocatalyst for efficient degradation of dyes and reduction of Cr(VI) in water, *RSC Adv.* 4 (2014) 19980–19986.
- [4] M. Shankar, S. Anandan, N. Venkatachalam, B. Arabindoo, V. Murugesan, Fine route for an efficient removal of 2,4-dichlorophenoxyacetic acid (2,4-D) by zeolite-supported  $\text{TiO}_2$ , *Chemosphere* 63 (2006) 1014–1021.
- [5] T.M. Silva, M.I. Stets, A.M. Mazzetto, F.D. Andrade, S.A.V. Pileggi, P.R. Favero, M.D. Cantu, E. Carrilho, P.I.B. Carneiro, M. Pileggi, Degradation of 2,4-D herbicide by microorganisms isolated from Brazilian contaminated soil, *Braz. J. Microbiol.* 38 (2007) 522–525.
- [6] P.H. Howard (Ed.), *Handbook of Environmental Fate and Exposure Data for Organic Chemicals—Vol. III, Pesticides*, Lewis Publishers, Chelsea, Mich, USA, 1991.
- [7] Y. Fu, T. Viraraghavan, Fungal decolorization of dye wastewaters: a review, *Bioresour. Technol.* 79 (2001) 251–262.

- [8] M.A. Farah, B. Ateeq, M.N. Ali, R. Sabir, W. Ahmad, Studies on lethal concentrations and toxicity stress of some xenobiotics on aquatic organisms, *Chemosphere* 55 (2004) 257–265.
- [9] Z. Chen, D. Li, W. Zhang, Y. Shao, T. Chen, M. Sun, X. Fu, Photocatalytic degradation of dyes by  $ZnIn_2S_4$  microspheres under visible light irradiation, *J. Phys. Chem. C* 113 (2009) 4433–4440.
- [10] W.J. Birge, J.A. Black, R. Kuehne, Effects of Organic Compounds on Amphibian Reproduction, 121, University of Kentucky, Water Resources Institute, Lexington, KY, 1980.
- [11] D.H. Pieper, V.A.P. Martins dos Santos, P.N. Golyshin, Genomic and mechanistic insights into the biodegradation of organic pollutants, *Curr. Opin. Biotechnol.* 15 (2004) 215–224.
- [12] Z. Aksu, E. Kabasakal, Batch adsorption of 2,4-dichlorophenoxy-acetic acid (2,4-D) from aqueous solution by granular activated carbon, *Sep. Purif. Technol.* 35 (2004) 223–240.
- [13] W.K. Lafi, Z. Al-Qodah, Combined advanced oxidation and biological treatment processes for the removal of pesticides from aqueous solutions, *J. Hazard. Mater.* 137 (2006) 489–497.
- [14] N.M. Julkapli, S. Bagheri, S.B.A. Hamid, Recent advances in heterogeneous photocatalytic decolorization of synthetic dyes, *Scientific World J.* 2014 (2014), <http://dx.doi.org/10.1155/2014/692307> (Article ID 692307, 25 pages).
- [15] J. Schneider, M. Matsuka, M. Takeuchi, J. Zhang, Y. Horiuchi, M. Anpo, D.W. Bahnemann, Understanding  $TiO_2$  photocatalysis: mechanisms and materials, *Chem. Rev.* 114 (2014) 9919–9986.
- [16] A. Fujishima, K. Honda, Electrochemical photolysis of water at a semiconductor electrode, *Nature* 238 (1972) 37–38.
- [17] T.S. Natarajan, K. Natarajan, H.C. Bajaj, R.J. Tayade, Energy efficient UV-LED source and  $TiO_2$  nanotube array-based reactor for photocatalytic application, *Ind. Eng. Chem. Res.* 50 (2011) 7753–7762.
- [18] S. Carbonaro, M.N. Sugihara, T.J. Strathmann, Continuous-flow photocatalytic treatment of pharmaceutical micropollutants: activity inhibition, and deactivation of  $TiO_2$  photocatalysts in wastewater effluent, *App. Catal. B: Environ.* 129 (2013) 1–12.
- [19] A. Fujishima, T.N. Rao, D.A. Tryk, Titanium dioxide photocatalysis, *J. Photochem. Photobiol. C: Photochem. Rev.* 1 (2000) 1–21.
- [20] E. Lee, Jin-Y. Hong, H. Kang, J. Jang, Synthesis of  $TiO_2$  nanorod-decorated graphene sheets and their highly efficient photocatalytic activities under visible-light irradiation, *J. Hazard. Mater.* 219–220 (2012) 13–18.
- [21] X. Zhang, T. Zhang, J. Ng, D.D. Sun, High-performance multifunctional  $TiO_2$  nanowire ultrafiltration membrane with a hierarchical layer structure for water treatment, *Adv. Funct. Mater.* 19 (2009) 3731–3736.
- [22] D. Zheng, Y. Xin, D. Ma, X. Wang, J. Wu, M. Gao, Preparation of graphene/ $TiO_2$  nanotube arrays photoelectrodes and their photocatalytic activities for the degradation of alachlor, *Catal. Sci. Technol.* 6 (2016) 1892–1902.
- [23] S.D. Perera, R.G. Mariano, K. Vu, N. Nour, O. Seitz, Y. Chabal, K.J. Balkus Jr., Hydrothermal synthesis of Graphene- $TiO_2$  nanotube composites with enhanced photocatalytic activity, *ACS Catal.* 2 (2012) 949–956.
- [24] N. Liu, X. Chen, J. Zhang, J.W. Schwank, A review on  $TiO_2$ -based nanotubes synthesized via hydrothermal method: formation mechanism, structure modification, and photocatalytic applications, *Catal. Today* 225 (2014) 34–51.
- [25] Y. Zhang, W. Zhu, X. Cui, W. Yao, T. Duan, One-step hydrothermal synthesis iron and nitrogen co-doped  $TiO_2$  nanotubes with enhanced visible-light photocatalytic activity, *CrystEngComm* 17 (2015) 8368–8376.
- [26] D.M. Chen, D. Yang, Q. Wang, Z.Y. Jiang, Effects of boron doping on photocatalytic activity and microstructure of titanium dioxide nanoparticles, *Ind. Eng. Chem. Res.* 45 (2006) 4110–4116.
- [27] W. Wang, D. Zhu, Z. Shen, J. Peng, J. Luo, X. Liu, One-Pot hydrothermal route to synthesize the Bi-doped anatase  $TiO_2$  hollow thin sheets with prior facet exposed for enhanced visible-light-driven photocatalytic activity, *Ind. Eng. Chem. Res.* 55 (2016) 6373–6383.
- [28] J.-J. Li, S.C. Cai, Z. Xu, X. Chen, J. Chen, H.P. Ji, J. Chen, Solvothermal syntheses of Bi and Zn co-doped  $TiO_2$  with enhanced electron-hole separation and efficient photodegradation of gaseous toluene under visible-light, *J. Hazard. Mater.* 325 (2017) 261–270.
- [29] M. Szkoda, K. Siuzdak, Anna Lisowska- Oleksiak, Non-metal doped  $TiO_2$  nanotube arrays for high efficiency photocatalytic decomposition of organic species in water, *Phys. E Low Dimens. Syst. Nanostruct.* 84 (2016) 141–145.
- [30] A. Pearson, H. Zheng, K. Kalantar-zadeh, S.K. Bhargava, V. Bansal, Decoration of  $TiO_2$  nanotubes with metal nanoparticles using Polyoxometalate as a UV-switchable reducing agent for enhanced visible and solar light photocatalysis, *Langmuir* 28 (2012) 14470–14475.
- [31] Z.W. Tong, D. Yang, Y.Y. Sun, Y. Tian, Z.Y. Jiang, In situ fabrication of  $Ag_3PO_4$ / $TiO_2$  nanotube heterojunctions with enhanced visible-light photocatalytic activity, *Phys. Chem. Chem. Phys.* 17 (2015) 12199–12206.
- [32] Q. Wang, X. Shi, E. Liu, J. Xu, J.C. Crittenden, Y. Zhang, Y. Cong, Preparation and photoelectrochemical performance of visible-light active  $AgI/TiO_2$ -NTs composite with rich  $\beta$ -Agl, *Ind. Eng. Chem. Res.* 55 (2016) 4897–4904.
- [33] B.K. Vijayan, N.M. Dimitrijevic, D. Finkelstein-Shapiro, J. Wu, K.A. Gray, Coupling titania nanotubes and carbon nanotubes to create photocatalytic nanocomposites, *ACS Catal.* 2 (2012) 223–229.
- [34] M.Q. Yang, N. Zhang, Y.J. Xu, Synthesis of fullerene-, carbon nanotube-, and graphene- $TiO_2$  nanocomposite photocatalysts for selective oxidation: a comparative study, *ACS Appl. Mater. Interfaces* 5 (2013) 1156–1164.
- [35] N. Zhang, M.Q. Yang, S. Liu, Y. Sun, Y.J. Xu, Waltzing with the versatile platform of graphene to synthesize composite photocatalysts, *Chem. Rev.* 115 (2015) 10307–10377.
- [36] Q. Huang, S. Tian, D. Zeng, X. Wang, W. Song, Y. Li, W. Xiao, C. Xie, Enhanced photocatalytic activity of chemically bonded  $TiO_2$ /graphene composites based on the effective interfacial charge transfer through the C-Ti bond, *ACS Catal.* 3 (2013) 1477–1485.
- [37] M. Sun, X. Ma, X. Chen, Y. Sun, X. Cui, Y. Lin, A nanocomposite of carbon quantum dots and  $TiO_2$  nanotube arrays: enhancing photoelectrochemical and photocatalytic properties, *RSC Adv.* 4 (2014) 1120–1127.
- [38] S. Umrao, S. Abraham, F. Theil, S. Pandey, V. Ciobota, P.K. Shukla, C.J. Rupp, S. Chakraborty, R. Ahuja, J. Popp, B. Dietzek, A. Srivastava, A possible mechanism for the emergence of an additional band gap due to a Ti-O-C bond in the  $TiO_2$ -graphene hybrid system for enhanced photodegradation of methylene blue under visible light, *RSC Adv.* 4 (2014) 59890–59901.
- [39] Y. Zhang, Z.R. Tang, X. Fu, Y.J. Xu,  $TiO_2$  graphene nanocomposites for gas-phase photocatalytic degradation of volatile aromatic pollutant: is  $TiO_2$ /graphene truly different from other  $TiO_2$  carbon composite materials? *ACS Nano* 4 (12) (2010) 7303–7314.
- [40] Y. Zhang, Z.R. Tang, X. Fu, Y.J. Xu, Engineering the unique 2D mat of graphene to achieve graphene- $TiO_2$  nanocomposite for photocatalytic selective transformation: what advantage does graphene have over its forebear carbon nanotube? *ACS Nano* 5 (9) (2011) 7426–7435.
- [41] M.Q. Yang, N. Zhang, M. Pagliaro, Y.J. Xu, Artificial photosynthesis over graphene-semiconductor composites. Are we getting better? *Chem. Soc. Rev.* 43 (2014) 8240–8254.
- [42] H. Zhang, X. Lv, Y. Li, Y. Wang, J. Li, P25-Graphene composite as a high performance photocatalyst, *ACS Nano* 4 (1) (2010) 380–386.
- [43] H. Yu, P. Xiao, J. Tian, F. Wang, J. Yu, Phenylamine-Functionalized rGO/ $TiO_2$  photocatalysts: spatially separated adsorption sites and tunable photocatalytic selectivity, *ACS Appl. Mater. Interfaces* 8 (2016) 29470–29477.
- [44] T.-D. Nguyen-Phan, V.H. Pham, J.S. Chung, M. Chhowalla, T. Asefa, W.-J. Kim, E.W. Shin, Photocatalytic performance of Sn-doped  $TiO_2$ /reduced graphene oxide composite materials, *Appl. Catal. A: Gen.* 473 (2014) 21–30.
- [45] W. Qian, P.A. Greaney, S. Fowler, S.-K. Chiu, A.M. Goforth, J. Jiao, Low-temperature nitrogen doping in ammonia solution for production of N-doped  $TiO_2$ -hybridized graphene as a highly efficient photocatalyst for water treatment, *ACS Sustainable Chem. Eng.* 2 (2014) 1802–1810.
- [46] Z. Chen, Y. Li, M. Guo, F. Xu, P. Wang, Y. Dub, P. Na, One-pot synthesis of Mn-doped  $TiO_2$  grown on graphene and the mechanism for removal of Cr(VI) and Cr(III), *J. Hazard. Mater.* 310 (2016) 188–198.
- [47] W. Yi, C. Yan, M.S. Hamdy, J. Baltrusaitis, G. Mul, Effects of bismuth addition and photo-deposition of platinum on (surface) composition morphology and visible light photocatalytic activity of sol-gel derived  $TiO_2$ , *Appl. Catal. B: Environ.* 154–155 (2014) 153–160.
- [48] Y. Chen, D. Chen, J. Chen, Q. Lu, M. Zhang, B. Liu, Q. Wang, Z. Wang, Facile synthesis of Bi nanoparticles modified  $TiO_2$  with enhanced visible light photocatalytic activity, *J. Alloy. Compd.* 651 (2015) 114–120.
- [49] Z. Bian, J. Ren, J. Zhu, S. Wang, Y. Lu, H. Li, Self-assembly of  $Bi_xTi_{1-x}O_2$  visible photocatalyst with core-shell structure and enhanced activity, *Appl. Catal. B: Environ.* 89 (2009) 577–582.
- [50] K. Lv, H. Zuo, J. Sun, K. Deng, S. Liu, X. Li, D. Wang, (Bi, C and N) codoped  $TiO_2$  nanoparticles, *J. Hazard. Mater.* 161 (2009) 396–401.
- [51] M.-C. Wu, J.-S. Chih, W.-K. Huang, Bismuth doping effect on  $TiO_2$  nanofibres for morphological change and photocatalytic performance, *CrystEngComm* 16 (2014) 10692–10699.
- [52] T. Kasuga, M. Hiramatsu, A. Hoson, T. Sekino, K. Niihara, Formation of titanium oxide nanotube, *Langmuir* 14 (1998) 3160–3163.
- [53] W.S. Hummers Jr., R.E. Offeman, Preparation of graphitic oxide, *J. Am. Chem. Soc.* 6 (1958) 1339.
- [54] U. Alam, A. Khan, W. Raza, A. Khan, D. Bahnemann, M. Munee, Highly efficient Y and V co-doped  $ZnO$  photocatalyst with enhanced dye sensitized visible light photocatalytic activity, *Catal. Today* 284 (2016) 169–178.
- [55] H. Li, X. Cui, A hydrothermal route for constructing reduced graphene oxide/ $TiO_2$  nanocomposites: enhanced photocatalytic activity for hydrogen evolution, *Int. J. Hydrogen Energy* 39 (2014) 19877–19886.
- [56] Y. Zhang, Z. Zhou, T. Chen, H. Wang, W. Lu, Graphene  $TiO_2$  nanocomposites with high photocatalytic activity for the degradation of sodium pentachlorophenol, *J. Environ. Sci.* 26 (2014) 2114–2122.
- [57] X. Pan, Y. Zhao, S. Liu, C.L. Korzeniewski, S. Wang, Z. Fan, Comparing graphene- $TiO_2$  nanowire and graphene- $TiO_2$  nanoparticle composite photocatalysts, *ACS Appl. Mater. Interfaces* 4 (2012) 3944–3950.
- [58] L. Wang, J. Fan, Z. Cao, Y. Zheng, Z. Yao, G. Shao, J. Hu, Fabrication of predominantly  $Mn^{4+}$ -doped  $TiO_2$  nanoparticles under equilibrium conditions and their application as visible-light photocatalysts, *Chemistry* 9 (2014) 1904–1912.
- [59] S. Rengaraj, X.Z. Li, P.A. Tanner, Z.F. Pan, G.K.H. Pang, Photocatalytic degradation of methylparathion—an endocrine disruptor by  $Bi^{3+}$ -doped  $TiO_2$ , *J. Mol. Catal. A: Chem.* 247 (2006) 36–43.
- [60] G. Li, J. Li, G. Li, G. Jiang, N and  $Ti^{3+}$  co-doped 3D anatase  $TiO_2$  superstructures composed of ultrathin nanosheets with enhanced visible light photocatalytic activity, *J. Mater. Chem. A* 3 (2015) 22073–22080.
- [61] Z. Bian, J. Ren, J. Zhu, S. Wang, Y. Lu, H. Li, Self-assembly of  $Bi_xTi_{1-x}O_2$  visible photocatalyst with core-shell structure and enhanced activity, *Appl. Catal. B: Environ.* 89 (2009) 577–582.
- [62] K. Lv, X. Li, K. Deng, J. Sun, X. Li, M. Li, Effect of phase structures on the photocatalytic activity of surface fluorinated  $TiO_2$ , *Appl. Catal. B: Environ.* 95 (2010) 383–392.

- [63] K. Lv, J. Yu, K. Deng, J. Sun, Y. Zhao, D. Du, M. Li, Synergistic effects of hollow structure and surface fluorination on the photocatalytic activity of titania, *J. Hazard. Mater.* 173 (2010) 539–543.
- [64] U.S. National Library of Medicine, Hazardous Substances Databank, Bethesda, Md USA, 1995.
- [65] P.H. Howard (Ed.), *Handbook of Environmental Fate and Exposure Data for Organic Chemicals—Vol. III, Pesticides*, Lewis Publishers, Chelsea, Mich, USA, 1991.
- [66] P.W.M. Augustijn-Beckers, R.D. Wauchope, A.G. Hornsby, SCS/ARS/CES pesticide properties database for environmental decision making II, additional compounds, *Rev. Environ. Contam. Toxicol.* 137 (1994) 1–82.
- [67] N.R. Khalid, E. Ahmed, Z. Hong, M. Ahmad, Synthesis and photocatalytic properties of visible light responsive La/TiO<sub>2</sub>-graphene composites, *Appl. Surf. Sci.* 263 (2012) 254–259.
- [68] Y. Wu, G. Lu, S. Li, The doping effect of Bi on TiO<sub>2</sub> for photocatalytic hydrogen generation and photodecolorization of rhodamine B, *J. Phys. Chem. C* 113 (2009) 9950–9955.
- [69] Y. Yang, T. Zhang, L. Le, X. Ruan, P. Fang, C. Pan, R. Xiong, J.W. J. Shi, Quick and facile preparation of visible light-driven TiO<sub>2</sub> photocatalyst with high absorption and photocatalytic activity, *Sci. Rep.* 4 (2014) 7045, <http://dx.doi.org/10.1038/srep07045>.
- [70] K. Zhou, Y. Zhu, X. Yang, X. Jiang, C. Li, Preparation of graphene?TiO<sub>2</sub> composites with enhanced photocatalytic activity, *New J. Chem.* 35 (2011) 353–359.
- [71] H. Zhang, L.-H. Guo, D. Wang, L. Zhao, B. Wan, Light-Induced efficient molecular oxygen activation on a Cu(II)-grafted TiO<sub>2</sub>/graphene photocatalyst for phenol degradation, *ACS Appl. Mater. Interfaces* 7 (2015) 1816–1823.
- [72] X. Wang, L. Zhi, K. Müllen, Conductive graphene electrodes for dye-sensitized solar cells, *Nano Lett.* 8 (2008) 323–327.
- [73] Q. Xiang, J. Yu, M. Jaroniec, Graphene-based semiconductor photocatalysts, *Chem. Soc. Rev.* 41 (2012) 782–796.
- [74] R. Qiao, M. Mao, E. Hu, Y. Zhong, J. Ning, Y. Hu, Facile formation of mesoporous BiVO<sub>4</sub>/Ag/AgCl heterostructured microspheres with enhanced visible-light photoactivity, *Inorg. Chem.* 54 (2015) 9033–9039.